

RESEARCH ARTICLE | JANUARY 03 2025

## Modeling correlated-noise in silicon spin qubit device

Guotong Cheng  ; Jing Guo  

APL Quantum 2, 016101 (2025)

<https://doi.org/10.1063/5.0216833>View  
OnlineExport  
Citation

### Articles You May Be Interested In

Effect of electron-nuclear spin interactions for electron-spin qubits localized in InGaAs self-assembled quantum dots

*J. Appl. Phys.* (January 2005)

Implementation of single-qubit gates with two rotations around axes in a plane

Flopping-mode spin qubit in a Si-MOS quantum dot

*Appl. Phys. Lett.* (March 2023)

# Modeling correlated-noise in silicon spin qubit device

Cite as: APL Quantum 2, 016101 (2025); doi: [10.1063/5.0216833](https://doi.org/10.1063/5.0216833)

Submitted: 1 May 2024 • Accepted: 11 December 2024 •

Published Online: 3 January 2025



[View Online](#)



[Export Citation](#)



[CrossMark](#)

Guotong Cheng and Jing Guo <sup>a</sup>

## AFFILIATIONS

Department of Electrical and Computer Engineering, University of Florida, Gainesville, Florida 32611, USA

<sup>a</sup>Author to whom correspondence should be addressed: [guoj@ufl.edu](mailto:guoj@ufl.edu)

## ABSTRACT

Silicon-based spin qubit platform is a promising candidate for the hardware realization of quantum computing. Charge noise, however, plays a critical role in limiting the fidelity and scalability of silicon-based quantum computing technologies. This work presents Green's transfer function approach to simulate the correlated noise power spectral density (PSD) in silicon spin qubit devices. The simulation approach relates the dynamics of the charge noise source of two-level fluctuators (TLFs) to the correlated noise of spin qubit device characteristics through a transfer function. It allows the noise auto-correlation and cross correlation between any pairs of physical quantities of interest to be systematically computed and analyzed. Because each spin qubit device involves only a small number of TLFs due to its nanoscale device size, the distribution of TLFs impacts the noise correlation significantly. In both a two-qubit quantum gate and a spin qubit array device, the charge noise shows strong cross correlation between neighboring qubits. The simulation results also reveal a phase-flipping feature of the noise cross-PSD between neighboring spin qubits, consistent with a recent experiment.

© 2025 Author(s). All article content, except where otherwise noted, is licensed under a Creative Commons Attribution (CC BY) license (<https://creativecommons.org/licenses/by/4.0/>). <https://doi.org/10.1063/5.0216833>

## I. INTRODUCTION

Noise is a showstopper for developing quantum computing technologies.<sup>1</sup> In semiconductor-spin-based quantum computing,<sup>2–4</sup> noise can stem from a variety of sources, including charge noise and nuclear magnetic noise.<sup>5–7</sup> Silicon can be isotopically purified to <sup>28</sup>Si with very high purity, in which nuclear dephasing is negligibly small compared to charge dephasing.<sup>2</sup> While significant progress has been achieved in reducing noise and improving the fidelity of the single-qubit and two-qubit quantum gates, noise is still the major factor that limits fidelity and scalability in silicon-based quantum computing.<sup>8–11</sup> In semiconductor spin qubits, the observed charge noise usually follows a 1/f-like power spectrum and is believed to be associated with two-level fluctuators (TLFs).<sup>5,12–14</sup> As the device size scales down and the integration density increases, the noises across neighboring qubits and quantum gates are increasingly correlated. Recent experimental work has investigated noise correlation spectrums in silicon spin qubits,<sup>15</sup> in which phase-flipping is observed in the noise correlation spectrum between two neighboring qubits. Along with experimental progress, developing physical models and understanding the noise correlation between neighboring spin qubits is important. Such understandings

are indispensable for developing strategies to mitigate noise for robust quantum computing systems based on silicon spin qubits.

In this work, we develop Green's transfer function approach to simulate the noise correlation spectrums of silicon-based spin qubits. The approach allows relating the dynamics of the noise source of TLFs to the correlated noise spectrums of the spin qubit devices through the transfer function. It provides a tool to systematically simulate and investigate both the auto-correlation and the cross correlation noise spectrums of silicon spin qubits. Using this simulation approach, we explore the correlated noise power spectral density (PSD) of the precession frequencies and exchange interaction in a two-qubit quantum gate device based on silicon. Due to the nanoscale device dimensionality of silicon spin qubit devices, only a few TLFs are involved. The results reveal strong noise cross correlation in silicon spin qubit devices and highlight the importance of the random discrete TLFs on the noise spectrum. The simulation shows the phase-flipping behavior of the cross correlation PSD between neighboring spin qubits as observed in a recent experiment.<sup>15</sup> This study contributes to the simulation method and understanding of correlated noise properties in silicon spin qubit devices, which is important for designing and scaling up silicon-spin-based quantum computing systems.

## II. APPROACH

The modeled device structures are shown in Fig. 1, which include both a two-qubit spin quantum gate in Fig. 1(a) and a one-dimensional spin qubit array in Fig. 1(b). Experimentally, both a SiGe–Si heterostructure and a silicon metal–oxide–semiconductor (MOS) structure have been used to fabricate silicon spin qubits.<sup>16</sup> In a SiGe–Si heterostructure, a thin silicon layer is sandwiched between SiGe layers. In a MOS structure, electrons are confined in the vertical direction by a potential well at the  $\text{SiO}_2$ –Si interface. The two quantum dots can be defined by applying gate voltages to the plunger gates (PGs), which operate the qubit pairs in the (1,1) electron number regime. The tunnel barriers between the QDs can be modulated by the barrier gate (BG). A thin oxide layer separates the gates with the top SiGe layer in the SiGe–Si heterostructure.

*Green's transfer function method:* We extend Green's transfer function method, which has been used in noise analysis of metal–oxide–semiconductor (MOS) FETs,<sup>17</sup> to noise analysis of semiconductor qubit devices. Charge fluctuation in TLFs creates a stochastic electric field perturbation to qubits and their exchange interactions. TLFs have been identified as the source of charge noise in semiconductor and superconductor qubit systems, although their microscopic physical origins remain a mystery.<sup>14,18,19</sup> For noise in a spin qubit system of  $N$  qubits, we define a vector of the physical quantities of interest  $P = [v_1, \dots, v_m, \dots, v_N, \dots, J_{mn}, \dots]$ ,

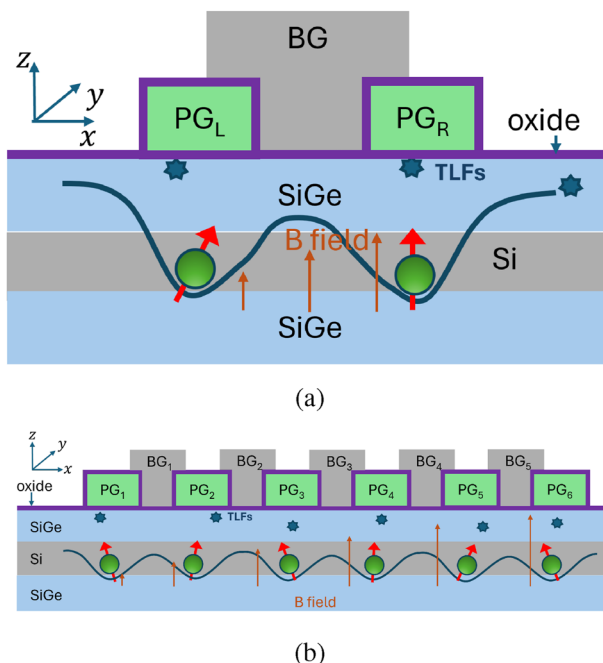


**FIG. 1.** Schematic structure of the modeled spin qubit device in silicon. (a) A two-qubit quantum gate. The QDs are defined by the left and right plunger gates,  $\text{PG}_L$  and  $\text{PG}_R$ . The tunnel barrier can be modulated by the barrier gate (BG). (b) A one-dimensional (1D) array of spin qubits. Both the PGs and BGs are shown. A silicon layer is confined between SiGe in a SiGe–Si heterostructure. The non-uniform magnetic field,  $B$  field, is denoted. The randomly distributed TLFs are shown schematically as stars.

where  $v_m$  is the precession frequency of each qubit, and  $J_{mn}$  is the exchange interaction (in a unit of Hertz) between a pair of qubits ( $m, n$ ). The autocorrelation function between the  $i_{th}$  and  $j_{th}$  elements of  $P$ ,  $R_{ij}(t) = \langle P_i(0)P_j(t) \rangle$ , forms a matrix. According to the Wiener–Khinchin theorem, its Fourier transform is the PSD  $S(f) = \mathcal{F}(R(t))$ , which can be computed from the PSD of the noise source  $K(f)$ ,

$$S(f) = G(f)K(f)G(f)^+, \quad (1)$$

where  $G(f)$  is the Green's transfer function matrix. At the low-frequency noise region,  $G(f)$  can be treated quasi-statically and is frequency-independent because the noise frequency scale associated with the fluctuation of TLFs is low. The diagonal element of  $S(f)$  gives the noise PSD of the physical quantities of interest. The off-diagonal elements compute the noise correlation between the  $i$ th and  $j$ th physical quantities of interest,

$$C_{ij}(f) = S_{ij}(f)/\sqrt{S_{ii}(f)S_{jj}(f)}. \quad (2)$$

*Model TLFs:* TLFs have been widely considered an important noise source in various quantum computing hardware platforms.<sup>14,19–21</sup> In superconductor qubits, TLFs are known to be approximately uniformly distributed across a wide range of frequencies. They possess both elastic and electric dipole moments, enabling them to interact with both mechanical deformation and electrical fields.<sup>19,20</sup> In semiconductor qubits, the dynamics of TLFs have been characterized and modeled.<sup>14,21</sup> Nonetheless, the precise physical nature of the TLFs in semiconductor qubits is still an open question.<sup>14</sup> In a simplified model, charge noise in semiconductors can be due to TLF defects capable of capturing and emitting charges.<sup>22,23</sup> The TLFs do not exchange charge with the QDs but can exchange charge with their environment, inducing carrier reservoirs of electrodes and nearby two-dimensional electron gas.<sup>14</sup> TLFs are not only limited to a whole electron charge fluctuation, in which a carrier is trapped and emitted, but also include dipolar fluctuations where a charge fluctuates between two positions within a double-well setup.<sup>24,25</sup> The TLFs are assumed to follow the dynamics of random telegraph noise (RTN) with a characteristic transition time of  $\tau_{Tk}$ .<sup>12,14,22</sup> The Fourier transform of its autocorrelation function of the TLF charge gives its power spectral density (PSD) in the form of a Lorentzian function with a corner frequency of  $f_{Tk} = 1/(2\pi\tau_{Tk})$ . The matrix elements of the noise source of the correlation has a Debye–Lorentzian spectrum,<sup>26</sup>

$$K_{kl}(f) = \frac{1}{2} \frac{\tau_{Tk}}{1 + (2\pi f \tau_{Tk})^2} \delta_{kl}, \quad (3)$$

where  $\delta_{kl}$  is the Kronecker delta, and  $\tau_{Tk}$  is the transition time of the  $k$ th TLF. Because the microscopic origin of the TLF is an open question, detailed physical knowledge of the transition time is absent. Assuming that the TLFs do not exchange charge with the QDs,<sup>25</sup> the transition time is determined more by the TLFs' interactions with their surroundings and each other rather than the QDs.<sup>25</sup> The transition rates of TLFs have exhibited distributions spanning various ranges and have shown dependence on gate voltages and temperatures, aspects that are not yet comprehensively understood.<sup>14,24</sup> In this study, we implement a random log-uniform distribution to represent the transition time of TLFs within specified ranges.<sup>25</sup>

*Model Green's transfer function:* TLFs result in a Coulombic field. A silicon spin qubit device has a nanoscale dimension. Only a small number of TLFs are involved for each device. For the  $k$ th TLF located at an in-plane position of  $(X_{Tk}, Y_{Tk})$  and a depth of  $d_{Tk}$  from the interface, by using the Thomas–Fermi (TF) approximation, the screened potential can be expressed as<sup>27,28</sup>

$$U_{Tk}(r) = \frac{1}{(2\pi)^2} \int_0^\infty q dq \int_0^{2\pi} d\theta V_{scr}(q) e^{iqrcos(\theta)}, \quad (4)$$

where

$$V_{scr}(q) = \frac{e^2}{2\epsilon_{si}} \frac{e^{-qd}}{q + q_{TF}}, \quad (5)$$

$r(x,y) = \sqrt{(x - X_{Tk})^2 + (y - Y_{Tk})^2}$ ,  $e$  is the elementary electron charge,  $\epsilon_{si}$  is the silicon dielectric constant, and  $q_{TF} \approx 0.67 \text{ nm}^{-1}$  is the TF screening wave vector.<sup>28</sup> The in-plane electrostatic force is computed as  $\vec{F}_{Tk}(x,y) = -\nabla U_{Tk}(x,y)$ . The potential at the  $i$ th QD can be evaluated as  $U_{ik} = \langle \psi_i(x,y) | U_{Tk}(x,y) | \psi_i(x,y) \rangle$ , and the force is computed as  $\vec{F}_{ik} = \langle \psi_i(x,y) | \vec{F}_{Tk}(x,y) | \psi_i(x,y) \rangle$ , where  $\psi_i(x,y)$  is the confined electron wave function. The wavefunction takes a Gaussian form<sup>29</sup> with a quadratic QD confinement potential  $V_{conf}(x,y) = \frac{1}{2} m^* \omega^2 ((x - x_c)^2 + (y - y_c)^2)$ , where the QD center is at  $(x_c, y_c)$ ,  $m^* = 0.19m_0$  is the in-plane effective mass of the (100) silicon layer, and  $m_0$  is the free electron mass, and a value of  $\hbar\omega = 5 \text{ meV}$  is used in this study, which results in a Gaussian form of the wave function with a radial characteristic length of  $l_{QD} = \sqrt{\hbar/(m^* \omega)} \approx 9.0 \text{ nm}$ .<sup>30</sup> This length scale defines the radial size of the confined electron wave function in a QD. The value is nominal and typical for a semiconductor QD, and varying the values does not change the qualitative conclusions. We consider randomly realized configurations with TLFs being  $>1.5l_{QD}$  away from the centers of the QDs, which results in a weak perturbation. The transfer Green's function can be treated by keeping the leading order perturbations.

We first model the transfer function term from the charge noise to a precession frequency. The electric field results in a displacement of the charge centroid of the confined electron. In the presence of a magnetic field gradient, it results in a fluctuation of the magnetic field. The in-plane displacement can be computed from the in-plane force,<sup>25</sup>

$$\delta\vec{r}_{ik} = \delta x_{ik}\hat{x} + \delta y_{ik}\hat{y} \approx \frac{\vec{F}_{ik}}{m^* \omega^2}. \quad (6)$$

In a device setup with the  $x$ -gradient of the magnetic field at the  $i$ th qubit dominating,  $\frac{\partial B_i}{\partial x} \gg \frac{\partial B_i}{\partial y}$ ,<sup>15</sup> the magnetic field variation due to position variation caused by the  $k$ th TLF charge is

$$\delta B_{ik} \approx \frac{\partial B_i}{\partial x} \delta x_{ik}. \quad (7)$$

In this study, we use a magnetic field gradient value of  $\frac{\partial B_i}{\partial x} = 0.1 \text{ mT/nm}$ , in the order of typical experimental value.<sup>6</sup> The charge noise of interest is low-frequency compared to the electrostatic response time. The Green's transfer function is treated as

frequency-independent. Its element between the fluctuation of the  $i$ th qubit precession frequency  $\delta\nu_i$  and  $k$ th TLF is determined by

$$G_{ik} = \frac{g_i \mu_B}{h} \delta B_{ik}, \quad (8)$$

where  $g_i$  is the  $g$ -factor,  $\mu_B$  is the Bohr magneton, and  $\delta B_{ik}$  is computed with Eq. (7).

After obtaining the transfer function for single qubit terms, we derive the transfer function term from the charge noise to the exchange coupling between neighboring qubits. If the Hubbard double-occupancy potential value is much larger than the tunnel coupling,  $U_H \gg t_c$ , the Schrieffer–Wolff transformation can be applied to obtain the Hamiltonian matrix in the computation subspace. The exchange part of the effective Hamiltonian between a neighboring pair of qubits  $(i, j)$  is  $H_{ex} = J_{ij} (\mathbf{S}_i \cdot \mathbf{S}_j - \frac{1}{4})$ ,<sup>31,32</sup> where  $\mathbf{S}_{i or j}$  is the spin operator, and the exchange interaction  $J_{ij}$  can be expressed as

$$J_{ij} = \frac{2t_{c,ij}^2}{U_{Hi} - \Delta_{ij}} + \frac{2t_{c,ij}^2}{U_{Hj} + \Delta_{ij}} = \frac{2t_{c,ij}^2 (U_{Hi} + U_{Hj})}{(U_{Hi} - \Delta_{ij})(U_{Hj} + \Delta_{ij})}, \quad (9)$$

where  $t_{c,ij}$  is the tunnel coupling,  $\Delta_{ij}$  is the detuning, and the Hubbard double-occupancy potential values are assumed to be equal  $U_{Hi} = U_{Hj} = U_H$ , which is insensitive to the TLF charge.<sup>31</sup> For a two-qubit quantum gate as shown in Fig. 1, there is only one exchange term between left and right QDs. The expression simplifies to

$$J_{ij} = \frac{4t_{c,ij}^2 U_H}{U_H^2 - \Delta_{ij}^2}. \quad (10)$$

The electric field by the TLF perturbs both the tunnel coupling  $t_{c,ij}$  and detuning  $\Delta$ .<sup>33</sup> Biasing the DQD structure at the sweet spot in which  $\Delta \ll U_H$  helps to reduce the impact of charge noise.<sup>34</sup> At this bias condition, the tunnel noise dominates<sup>33</sup>

$$\delta J_{ij} \approx \frac{2J_{ij} \delta t_{c,ij}}{t_{c,ij}}. \quad (11)$$

The tunnel coupling  $t_{c,ij}$  depends on the tunnel barrier height and thickness between neighboring qubits. The tunnel coupling between two neighboring qubits can be numerically computed with a Schrödinger–Poisson solver.<sup>35</sup> The numerically computed tunnel coupling value can be described by an analytical expression in the form of the WKB approximation, which is expressed as<sup>33,35</sup>

$$t_{c,ij} = t_{c0} \exp\left(-\frac{\sqrt{2qm^* E_{b,ij}}}{\hbar} L_{s,ij}\right), \quad (12)$$

where  $E_{b,ij}$  is the barrier height,  $L_{s,ij}$  is the spacing between the double quantum dots,  $q$  is the elementary electron charge, and  $t_{c0}$  is a tunnel coupling parameter independent of  $E_{b,ij}$  and  $L_{s,ij}$ . The tunnel coupling parameter can be obtained by fitting Eq. (12) to the numerical simulation results of the tunnel coupling values at different QD spacings and barrier heights.<sup>35</sup> The extracted pre-coefficient  $t_{c0}$  depends on the semiconductor material and carrier type.<sup>35</sup> For silicon electron tunnel coupling, the pre-coefficient value is in the order of  $t_{c0} \approx 10 \text{ meV}$ . The perturbation of a TLF on the barrier

height  $E_b$  is small. The barrier height in the typical operation condition is in the order of  $\sim 10$  meV, while the perturbation to the barrier height for a TLF with an in-plane distance of  $> 10$  nm is in the order of  $\sim 10 \mu\text{eV}$  or smaller, which is orders of magnitude smaller than a typical tunnel barrier height. The fluctuation of the tunnel coupling can be approximately expressed as

$$\frac{\delta t_{c,ij}}{t_{c,ij}} \approx \left( -\frac{\sqrt{2qm^*E_{b,ij}}}{\hbar} L_{s,ij} \right) \left( \frac{\delta L_{s,ij}}{L_{s,ij}} + \frac{\delta E_{b,ij}}{2E_{b,ij}} \right). \quad (13)$$

The  $k$ th TLF perturbs the interdot spacing and the tunnel spacing,

$$\delta L_{s,ij} = \delta x_{ik} - \delta x_{jk} = \frac{F_{x,ik}}{m^* \omega_i^2} - \frac{F_{x,jk}}{m^* \omega_j^2}, \quad (14)$$

where  $F_x$  is the  $x$ -component of the electrostatic force. The change in the barrier height due to the TLF charge is computed by averaging over the tunneling path,

$$\delta E_{b,ij} = \frac{\int_{x_i}^{x_j} U_{Tk}(x, y=0) dx}{x_j - x_i}. \quad (15)$$

The matrix element of Green's transfer function between an exchange interaction term  $\delta J_{ij}$  and the  $k$ th TLF is obtained by substituting Eq. (13) into Eq. (11),

$$G_{J_{ij},k} = 2J_{ij} \left( -\frac{\sqrt{2qm^*E_{b,ij}}}{\hbar} L_{s,ij} \right) \left( \frac{\delta L_{s,ij}}{L_{s,ij}} + \frac{\delta E_{b,ij}}{2E_{b,ij}} \right), \quad (16)$$

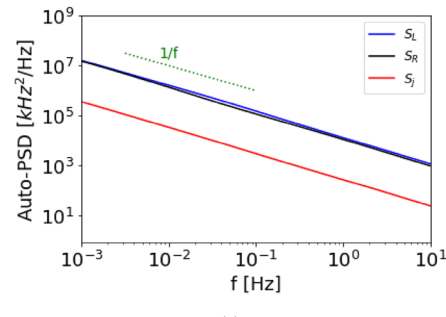
where  $\delta L_{s,ij}$  is computed by Eq. (14) and  $\delta E_{b,ij}$  is computed from Eq. (15).

### III. RESULTS

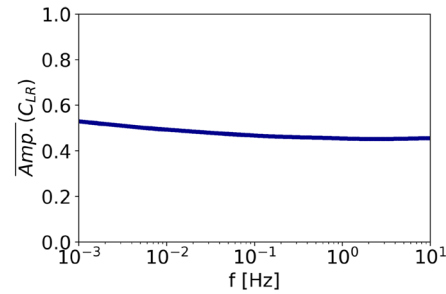
We first apply the transfer Green's function method to investigate noise correlations in the two-qubit quantum gate device as shown in Fig. 1. The spacing between the two QD centers is  $L_S = 40$  nm. Both the Si layer and SiGe layer are assumed to have a thickness of 10 nm. We examine the noise auto-correlation and cross correlation of the precession rates of the left and right qubits,  $\nu_L$  and  $\nu_R$ , respectively, and the exchange interaction between the qubits,  $J$ . For the device, the vector of physical quantities of interest is  $P = [\nu_L, \nu_R, J]$ . The auto-PSD values are extracted from the diagonal entries of  $S(f)$  in Eq. (1) and are denoted using  $S_L$ ,  $S_R$ , and  $S_J$  for  $\nu_L$ ,  $\nu_R$ , and  $J$ , respectively. The cross correlation values are obtained from Eq. (2) and are denoted using the symbol  $C$  with subscripts.

In an isotopically purified Si<sup>28</sup>, the charge noise dominates. The nuclear magnetic mechanism is weak, which can lead to a corresponding dephasing time  $T_2^{nu} > 100 \mu\text{s}$ . Spin-orbit coupling is also weak in silicon.<sup>2</sup> We first focus on the case with charge noise only. The distribution of TLFs is randomly generated. To explore the statistical average values. We stochastically generate the TLF configurations with a density of  $N_{\text{TLF}} = 4 \times 10^{11}/\text{cm}^2$ ,<sup>36</sup> stochastically uniformly distributed in the capping SiGe layer in the thickness direction.

To explore the statistical average over random realizations of TLF configurations, we realize  $N_{\text{config}} = 8000$  configurations of



(a)



(b)

**FIG. 2.** (a) The expectation value of the auto-PSDs of the precession frequencies,  $S_L$  (blue solid) and  $S_R$  (black solid), and the exchange interaction  $S_J$  (red solid), over random TLF distributions. A reference line of  $1/f$  scaling is also shown (green dot). (b) The amplitude of the expectation value of the cross-PSD,  $C_{LR}$ , between the precession frequencies of two qubits. The expectation values are computed by using 8000 random realizations of the TLF distributions.

the TLFs stochastically and compute the expectation values of noise correlation spectrums by averaging over these configurations. Figure 2(a) shows that the expected auto-PSDs of the precession frequencies of two qubits are essentially equal and show a  $1/f$  noise scaling behavior. Each individual TLF produces a Lorentzian power spectrum. In calculating the expectation over a larger number of random TLF realizations, summing and averaging over Lorentzian with different corner frequency values leads to a  $1/f$  scaling behavior of the expectation value. Similarly, the expectation value of the auto-PSD of the exchange interaction shows a clear  $1/f$  scaling behavior. The cross correlation between two neighboring qubits is characterized by the cross-PSD of the precession frequencies of two QDs. Figure 2(b) shows the expectation value of the amplitude of the cross-PSD over all TLF relations is  $\bar{A} \approx 0.5$ , and it is nearly frequency-independent. The cross-PSD amplitude is bounded between 0, which corresponds to no correlation, and 1, which corresponds to the case of fully correlated or anticorrelated. The expectation value of the cross-PSD amplitude indicates that the correlation is strong on average. At a specified frequency, the phases of the cross-PSD of various random realizations take a random binary value of 0, which indicates in-phase, or  $\pi$ , which indicates out-of-phase, and the average phase value is  $\pi/2$ .

Next, we examine the noise correlation of one randomly realized configuration of TLFs. Figure 3(a) shows the noise auto-PSD  $S_L$  of the precession frequency of the left qubit. Figure 3(b) shows the

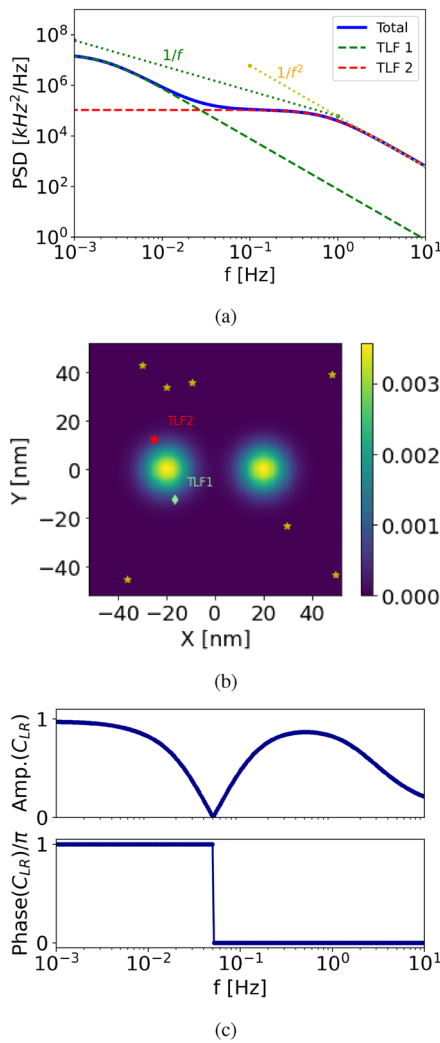


**FIG. 3.** Noise auto-PSD of the spin qubit precession frequency at the left QD  $S_L$  (solid) for the TLF configuration in (b). The auto-PSDs due to charge in TLF 1 and TLF 2, as denoted in (b), are shown by the green and red dashed lines, respectively, with a color bar in the unit of  $\text{nm}^{-2}$ .  $1/f$  and  $1/f^2$  scaling lines are also shown by the green and yellow dotted lines. (b) A randomly realized TLF configuration and the pseudo-color plot of the electron probability density. All TLF charges are shown by scattered symbols. Two TLF charges with dominant contributions to the noise correlations in the frequency range of interest are denoted as the white diamond (TLF 1) and the red circle (TLF 2), and the rest of the TLF charges are denoted as yellow stars. (c) The amplitude (top) and phase (bottom) of the cross correlation  $C_{LR}$  between the precession frequencies of two qubits. The modeled device structure is shown in Fig. 1. The QD spacing is  $L_S = 40 \text{ nm}$  with the QD centers located at  $(\pm 20 \text{ nm}, 0)$ .

top view of the TLF distribution and the electron probability density of two spin qubits. We also simulated the PSD due to an individual TLF only, as shown by the green dashed line for TLF 1 and the red dashed line for TLF 2 in Fig. 3(a). The results show that the total PSD can be well described by the sum of the PSDs from these two contributors. Each TLF charge results in a Lorentzian PSD, which is nearly constant at a frequency lower than its corner frequency and scales as

$1/f^2$  at high frequencies. The sum of the contributions by TLFs 1 and 2 results in a  $1/f$  scaling of their values at the corner frequencies, as shown by the slope of the green dot line in Fig. 3(a). These two TLFs have a dominant contribution because they have corner frequencies in the frequency range of interest. A recent experiment examined the impact of an individual TLF on a silicon spin qubit.<sup>14</sup> In the silicon spin qubits for a given frequency range, there can be only a single TLF playing a dominant role because of the small number of TLFs and the spread of their frequency ranges. As shown in Fig. 3(a), in the frequency range around  $10^{-3}$  to  $10^{-2}$  Hz, the individual TLF 1 has a dominant contribution to the total noise PSD, and in the frequency range around  $10^{-1}$  to  $10^0$  Hz, the individual TLF 2 has a dominant contribution. In the frequency range around  $10^{-2}$  to  $10^{-1}$  Hz, both TLF1 and TLF2 contribute. The spin qubit probes the fluctuation of only one or two TLFs in the frequency range examined.

Noise correlation for a pair of neighboring qubits has been experimentally investigated,<sup>15</sup> which shows strong cross correlation and a phase-flipping feature from out-of-phase to in-phase in an explored frequency range. We next investigate the cross correlation of noise between two qubits. The cross-PSD  $C_{LR}$  between  $v_L$  and  $v_R$  is shown in Fig. 3(c). The results show a qualitative feature drastically different from the expectation value as shown in Fig. 2(b), which highlights the importance of a small number of random discrete TLF charges. The cross-PSD flips from out-of-phase with  $\phi = \pi$  at lower frequencies to in-phase with  $\phi = 0$  at higher frequencies. The amplitude indicates strong cross correlation, with the peak value approaching the maximum value of 1. The reason for the

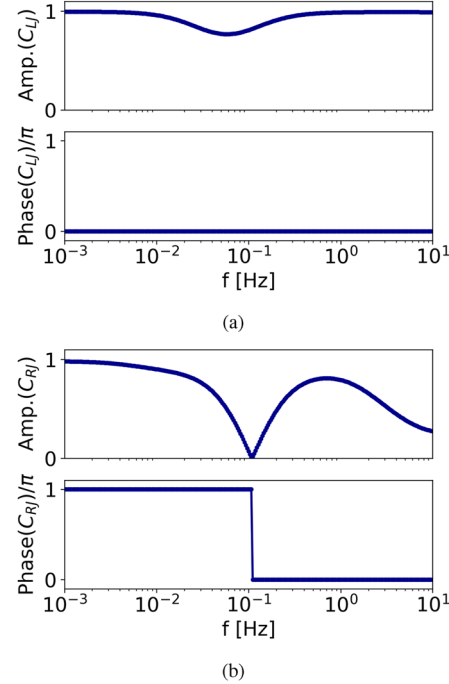


**FIG. 4.** The amplitude (top) and phase (bottom) of (a) the cross-PSD  $C_{LJ}$  between  $v_L$  and  $J$ , and (b) the cross-PSD  $C_{RJ}$  between  $v_R$  and  $J$ . The TLF configuration is shown in Fig. 3(b).

out-of-phase to in-phase transition is explained as follows: As discussed before, TLFs 1 and 2, as shown in Fig. 3(b), have dominant contributions among all TLFs due to their closeness in space to the quantum dot centroids. TLF 1 is located at an  $x$  position between the charge centroids of the left and right QDs. The charge of the TLF 1 results in electrostatic forces that move two qubits' charges along the opposite  $x$  directions. In contrast, TLF 2 is located to the left of both QDs. Its charge results in electrostatic forces that move both qubit charges along the same  $x$  direction. In the presence of a magnetic field gradient along the  $x$  direction, the cross-PSD due to TLF 1 is out-of-phase, and that due to TLF 2 is in-phase. As shown in Fig. 3(a), TLF 1 has a lower corner frequency and is more dominant at lower frequencies, and TLF 2 is more dominant at higher frequencies. As the frequency increases, the cross-PSD flips from out-of-phase due to the dominance of the slower TLF 1 to in-phase due to the dominance of the faster TLF 2. Although the random nature of TLFs makes it difficult for a quantitative comparison between theory and experiment, the phase-flipping phenomenon in a correlated noise spectrum has also been experimentally observed in a pair of silicon spin qubits.<sup>15</sup> The qualitative feature of the cross-PSD shown here is similar to an experimental observation in the experiment.<sup>15</sup>

The cross-PSDs between the precession frequencies and the exchange interaction are investigated next. Figure 4 plots the cross-PSD between the spin qubit precession frequencies and the exchange interaction  $J$ , for the same TLF configuration in Fig. 3. The amplitude of cross-PSD values indicates a strong noise cross correlation between the two-qubit exchange coupling and single-qubit precession frequencies. The left spin qubit stays in-phase with the exchange interaction in the frequency range explored, as shown in the bottom

panel of Fig. 4(a). In contrast, the right qubit switches from out-of-phase to in-phase, as shown in the bottom panel of Fig. 4(b). This is consistent with Fig. 3(c). As the noise of  $\nu_L$  stays in phase with the noise of the exchange interaction  $J$ , the noise of  $\nu_R$  goes through a phase-transition from out-of-phase to in-phase with the noises of both  $\nu_L$  and  $J$ .

In natural silicon, the nuclear magnetic noise is significantly stronger than in isotopically purified Si<sup>28</sup>. The nuclear magnetic noise is due to a localized Overhauser field.<sup>2</sup> The Overhauser field results in uncorrelated magnetic noise on two qubit spins, and it does not affect the exchange interaction. We model the impact of the additional nuclear magnetic noise mechanism by adding a diagonal PSD matrix  $S^{nu}(f)$  to the previously calculated noise PSD matrix of the charge noise  $S(f)$  in Eq. (1) to obtain the total noise PSD matrix,  $S^{tot}(f) = S^{nu}(f) + S(f)$ . For the physical quantities of interest,  $P = [\nu_1, \dots, \nu_m, \dots, \nu_N, \dots, J_{mn}, \dots]$ , the nuclear magnetic noise is modeled phenomenologically with a scaling of  $1/f^\alpha$ , where the exponent  $\alpha$  is typically in the range of  $1 \leq \alpha \leq 2$ .<sup>37</sup> The diagonal entries corresponding to the precession frequency of a spin qubit describe the magnetic noise of spin precession frequencies,

$$S_{ii}^{nu}(f) = \begin{cases} A^{nu}/f^\alpha & \text{if } i \leq N, \\ 0, & \text{otherwise,} \end{cases} \quad (17)$$

where  $A^{nu}$  determines the strength of the noise. This simple phenomenological model is useful to shed light on how the additional magnetic noise impacts noise correlation PSDs.

Figure 5 shows the auto-PSD and cross-PSD with various strengths of nuclear noise. Two scaling power coefficient  $\alpha$  values in

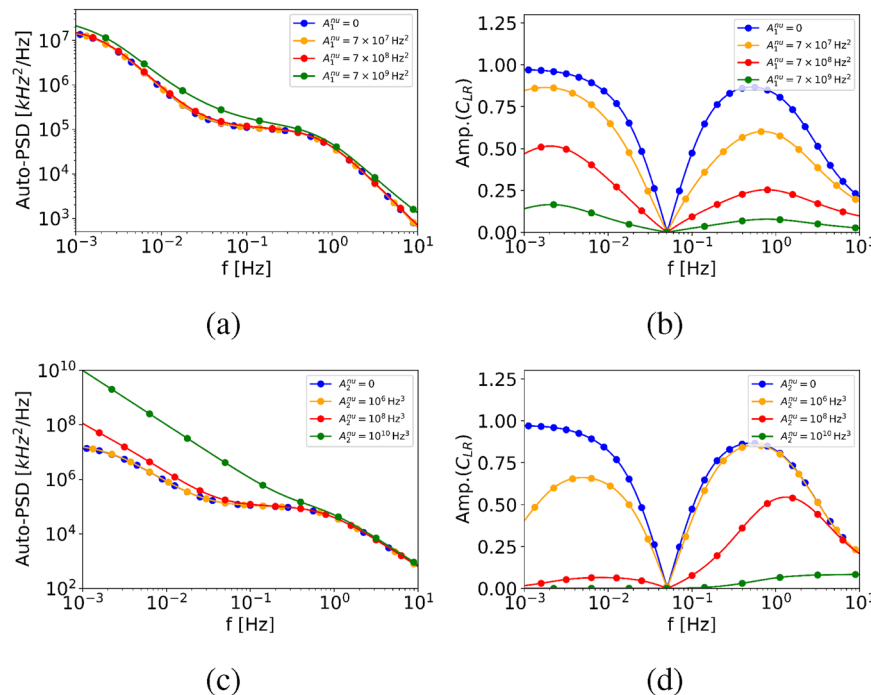


**FIG. 5.** Impact on the noise correlation PSDs after including additional noise with either  $1/f$  scaling in (a) and (b) or  $1/f^2$  scaling in (c) and (d). (a) The auto-PSD  $S_L(f)$  of the precession frequency  $\nu_L$  and (b) the amplitude of the cross-PSD  $C_{LR}$  between  $\nu_L$  and  $\nu_R$  for various strengths of nuclear magnetic noise with a PSD of  $A_1^{nu}/f$ , where  $A_1^{nu} = 0$  (blue),  $A_1^{nu} = 7 \times 10^7 \text{ Hz}^2$  (orange),  $A_1^{nu} = 7 \times 10^8 \text{ Hz}^2$  (red), and  $A_1^{nu} = 7 \times 10^9 \text{ Hz}^2$  (green). (c) The auto-PSD  $S_L(f)$  of the precession frequency  $\nu_L$  and (d) the amplitude of the cross-PSD  $C_{LR}$  between  $\nu_L$  and  $\nu_R$  for various strengths of nuclear magnetic noise with a PSD of  $A_2^{nu}/f^2$ , where  $A_2^{nu} = 0$  (blue),  $A_2^{nu} = 10^6 \text{ Hz}^3$  (orange),  $A_2^{nu} = 10^8 \text{ Hz}^3$  (red), and  $A_2^{nu} = 10^{10} \text{ Hz}^3$  (green). In (a) and (c), the orange and blue lines nearly overlap. The TLF configuration is shown in Fig. 3(b).

Eq. (17) are investigated to cover the boundary values of  $1 \leq \alpha \leq 2$ . Figures 5(a) and 5(b) show the results of  $\alpha = 1$ , and Figs. 5(c) and 5(d) show the results of  $\alpha = 2$ . The solid lines show the baseline without nuclear magnetic noise. The results indicate that the cross correlation PSDs in Figs. 5(b) and 5(d) are more sensitive

to the additional nuclear magnetic noise compared to the auto-correlation PSDs in Figs. 5(a) and 5(c). For relatively weak added nuclear magnetic noises as shown by the black lines in Fig. 5, the impact on the auto-correlation PSDs, as shown in Figs. 5(a) and 5(c), is negligibly small. However, the impacts on the cross correlation between spin precession frequencies are already considerable, as shown in Figs. 5(b) and 5(d). A large value of cross-PSDs indicates that the charge noise is more dominant than the nuclear magnetic noise.

Spin qubit arrays have been demonstrated to increase the qubit count for quantum processors by only considering charge noise.<sup>38</sup> We next investigate noise correlations in a one-dimensional (1D) spin qubit array. The modeled device structure consists of  $N_{\text{QD}} = 6$  qubits with the nearest neighbor distance of 40 nm, as schematically shown in Fig. 1(b). Figure 6 plots the amplitude of  $C_{ij}(f)$  in Eq. (2) between a pair of precession frequencies or a pair of exchange interactions. The diagonal entry is always 1, and the off-diagonal entry indicates the amplitude of cross correlations. Figure 6(a) shows the noise correlation  $C(f)$  in Eq. (2) between the precession frequencies of the spin qubits, and Fig. 6(b) shows the noise correlation between the exchange interactions. The diagonal entries have a maximum magnitude of 1. The results indicate strong cross correlations in a spin qubit array for both the precession frequencies and exchange interactions among neighboring qubits in a spin qubit array. Similar to the noise cross correlations in the two-qubit quantum gate, the amplitudes of the correlations are also dependent on the frequency. In general, Figs. 6(a) and 6(b) indicate that cross correlation values in the off-diagonal entries nearer to the diagonal tend to be stronger. This observation implies that the cross correlation between spins in a scaled spin qubit array, particularly among pairs situated closer spatially, is strong. The results also suggest that the cross correlation beyond the nearest neighbors, shown in the figures as the second off-diagonal and beyond, can be significant.

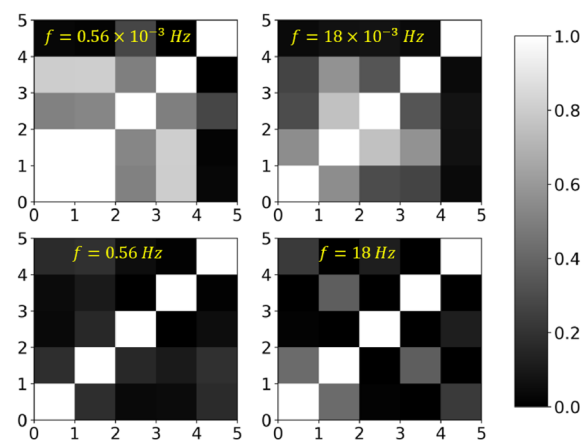
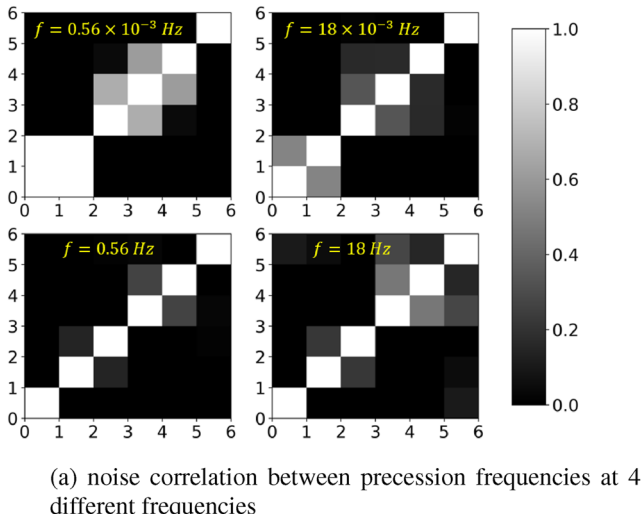


**FIG. 6.** Noise correlation amplitude,  $|C_{ij}(f)|$  in Eq. (2), in a 1D spin qubit array with a randomly realized TLF configuration. Pseudo-color plots of (a) noise correlation  $C_{ij}(f)$  between the precession frequencies of the  $i$ th and  $j$ th qubits  $v_i$  and  $v_j$ , where the indices  $1 \leq i, j \leq N_{\text{QD}}$  are shown as the  $x$  and  $y$  axis values, and (b) noise correlation  $C_{J_m, J_n}(f)$  between exchange interactions  $J_{m,m+1}$  and  $J_{n,n+1}$ , where  $J_{m,m+1}$  or  $J_{n,n+1}$  is the exchange between a pair of neighboring qubits in the 1D array. The indices  $1 \leq m, n \leq N_{\text{QD}} - 1$  are shown as the vertical and horizontal axis values. In both (a) and (b), the noise correlation is sampled at four frequency values:  $f = 0.56 \times 10^{-3}$  Hz (top-left),  $18 \times 10^{-3}$  Hz (top-right),  $0.56$  Hz (bottom-left), and  $18$  Hz (bottom-right). The qubit array structure is schematically shown in Fig. 1(b), with  $N_{\text{QD}} = 6$  spin qubits and nearest neighbor spacing of 40 nm. The spin qubits are ordered from 1 to  $N_{\text{QD}}$  from left to right in the array. The randomly realized TLF configuration has a density of  $N_{\text{TLF}} = 4 \times 10^{11}/\text{cm}^2$ .

#### IV. DISCUSSIONS AND CONCLUSIONS

Noise imposes a major challenge for improving fidelity and scaling up qubit counts in semiconductor-based quantum computing. We extend Green's transfer function approach, previously used to simulate noise PSDs in conventional semiconductor devices, to model noise correlation in silicon spin qubit devices. The modeling procedure of relating the dynamics of the charge noise source to the noise correlation PSDs of precession frequencies and exchange interactions in a silicon spin qubit device is described. While previous modeling works focus more on explaining specific experiments,<sup>15,39</sup> this work presents a general noise modeling framework based on the transfer Green's function method for spin qubit systems. The transfer Green's function approach allows treating multiple noise sources from various noise mechanisms and their correlations in the noise source spectrum matrix  $K$ . It can incorporate the physical mechanisms of propagating from various noise sources to the noise observations in the transfer Green's function matrix. Furthermore, the noise auto-correlation and cross correlation between any pairs of observables can be directly obtained from the noise correlation matrix obtained by propagating the noise source through the transfer Green's function. The approach, therefore, provides a scalable method that can be conveniently applied to

calculate noise correlations in larger spin qubit systems, arranged in either one-dimension or two-dimensions.

The modeling results reveal strong noise cross correlations in an array of spin qubits. Due to the nanometer scale device size and the small number of TLFs involved, the discrete and random nature of the TLFs plays an important role in silicon spin qubit devices. The simulation results indicate that the noise correlation spectrum densities of a random TLF configuration differ considerably from the statistical expectation values. The results also provide insights into the phase-flipping phenomena of the noise cross-PSD in a silicon spin qubit device observed experimentally. The modeling approach developed is useful for calculating and comprehending noise correlations within semiconductor spin qubit systems, which can be an important step toward devising future techniques to mitigate correlated quantum noise.

## ACKNOWLEDGMENTS

This work was supported by NSF Grant Nos. 2007200 and 2142552.

## AUTHOR DECLARATIONS

### Conflict of Interest

The authors have no conflicts to disclose.

### Author Contributions

**Guoting Cheng:** Data curation (equal); Methodology (equal); Visualization (equal); Writing – original draft (equal); Writing – review & editing (equal). **Jing Guo:** Conceptualization (lead); Formal analysis (equal); Funding acquisition (lead); Investigation (equal); Methodology (equal); Supervision (lead); Visualization (equal); Writing – original draft (equal); Writing – review & editing (equal).

## DATA AVAILABILITY

The data that support the findings of this study are available from the corresponding author upon reasonable request.

## REFERENCES

- <sup>1</sup>A. A. Clerk, M. H. Devoret, S. M. Girvin, F. Marquardt, and R. J. Schoelkopf, “Introduction to quantum noise, measurement, and amplification,” *Rev. Mod. Phys.* **82**(2), 1155 (2010).
- <sup>2</sup>G. Burkard, T. D. Ladd, A. Pan, J. M. Nichol, and J. R. Petta, “Semiconductor spin qubits,” *Rev. Mod. Phys.* **95**(2), 025003 (2023).
- <sup>3</sup>M. A. Eriksson, M. Friesen, S. N. Coppersmith, R. Joynt, L. J. Klein, K. Slinker, C. Tahan, P. Mooney, J. Chu, and S. Koester, “Spin-based quantum dot quantum computing in silicon,” *Quantum Inf. Process.* **3**, 133–146 (2004).
- <sup>4</sup>L. M. Vandersypen and M. A. Eriksson, “Quantum computing with semiconductor spins,” *Phys. Today* **72**(8), 38–45 (2019).
- <sup>5</sup>E. J. Connors, J. Nelson, H. Qiao, L. F. Edge, and J. M. Nichol, “Low-frequency charge noise in Si/SiGe quantum dots,” *Phys. Rev. B* **100**(16), 165305 (2019).
- <sup>6</sup>J. Yoneda, K. Takeda, T. Otsuka, T. Nakajima, M. R. Delbecq, G. Allison, T. Honda, T. Kodera, S. Oda, Y. Hoshi *et al.*, “A quantum-dot spin qubit with coherence limited by charge noise and fidelity higher than 99.9%,” *Nat. Nanotechnol.* **13**(2), 102–106 (2018).
- <sup>7</sup>U. Güngördu and J. Kestner, “Indications of a soft cutoff frequency in the charge noise of a Si/SiGe quantum dot spin qubit,” *Phys. Rev. B* **99**(8), 081301 (2019).
- <sup>8</sup>M. Veldhorst, C. Yang, J. Hwang, W. Huang, J. Dehollain, J. Muñoz, S. Simmons, A. Laucht, F. Hudson, K. M. Itoh *et al.*, “A two-qubit logic gate in silicon,” *Nature* **526**(7573), 410–414 (2015).
- <sup>9</sup>M. T. Mądzik, S. Asaad, A. Youssry, B. Joecker, K. M. Rudinger, E. Nielsen, K. C. Young, T. J. Proctor, A. D. Baczewski, A. Laucht *et al.*, “Precision tomography of a three-qubit donor quantum processor in silicon,” *Nature* **601**(7893), 348–353 (2022).
- <sup>10</sup>S. G. Philips, M. T. Mądzik, S. V. Amitonov, S. L. de Snoo, M. Russ, N. Kalhor, C. Volk, W. I. Lawrie, D. Brousse, L. Tryputen *et al.*, “Universal control of a six-qubit quantum processor in silicon,” *Nature* **609**(7929), 919–924 (2022).
- <sup>11</sup>X. Xue, M. Russ, N. Samkharadze, B. Undseth, A. Sammak, G. Scappucci, and L. M. Vandersypen, “Quantum logic with spin qubits crossing the surface code threshold,” *Nature* **601**(7893), 343–347 (2022).
- <sup>12</sup>L. Kranz, S. K. Gorman, B. Thorgrimsson, Y. He, D. Keith, J. G. Keizer, and M. Y. Simmons, “Exploiting a single-crystal environment to minimize the charge noise on qubits in silicon,” *Adv. Mater.* **32**(40), 2003361 (2020).
- <sup>13</sup>B. Paquet Wuett, D. Degli Esposti, A.-M. J. Zwerver, S. V. Amitonov, M. Botifoll, J. Arbiol, L. M. K. Vandersypen, M. Russ, G. Scappucci, and G. Scappucci, “Reducing charge noise in quantum dots by using thin silicon quantum wells,” *Nat. Commun.* **14**(1), 1385 (2023).
- <sup>14</sup>F. Ye, A. Ellaboudy, D. Albrecht, R. Vudatha, N. T. Jacobson, and J. M. Nichol, “Characterization of individual charge fluctuators in Si/SiGe quantum dots,” *Phys. Rev. B* **110**, 235305 (2024).
- <sup>15</sup>J. Yoneda, J. Rojas-Arias, P. Stano, K. Takeda, A. Noiri, T. Nakajima, D. Loss, and S. Tarucha, “Noise-correlation spectrum for a pair of spin qubits in silicon,” *Nat. Phys.* **19**(12), 1793–1798 (2023).
- <sup>16</sup>A. Saraiya, W. H. Lim, C. H. Yang, C. C. Escott, A. Laucht, and A. S. Dzurak, “Materials for silicon quantum dots and their impact on electron spin qubits,” *Adv. Funct. Mater.* **32**(3), 2105488 (2022).
- <sup>17</sup>F.-C. Hou, G. Bosman, and M. E. Law, “Simulation of oxide trapping noise in submicron n-channel MOSFETs,” *IEEE Trans. Electron Devices* **50**(3), 846–852 (2003).
- <sup>18</sup>C. Wang, C. Axline, Y. Y. Gao, T. Brecht, Y. Chu, L. Frunzio, M. Devoret, and R. J. Schoelkopf, “Surface participation and dielectric loss in superconducting qubits,” *Appl. Phys. Lett.* **107**(16), 162601 (2015).
- <sup>19</sup>M. Chen, J. C. Owens, H. Puterman, M. Schäfer, and O. Painter, “Phonon engineering of atomic-scale defects in superconducting quantum circuits,” *Sci. Adv.* **10**(37), eado6240 (2024).
- <sup>20</sup>C. Müller, J. H. Cole, and J. Lisenfeld, “Towards understanding two-level-systems in amorphous solids: Insights from quantum circuits,” *Rep. Prog. Phys.* **82**(12), 124501 (2019).
- <sup>21</sup>A. Ayachi, W. B. Chouikha, S. Jaziri, and R. Bennaceur, “Telegraph noise effects on two charge qubits in double quantum dots,” *Phys. Rev. A* **89**(1), 012330 (2014).
- <sup>22</sup>E. Paladino, Y. Galperin, G. Falci, and B. Altshuler, “1/f noise: Implications for solid-state quantum information,” *Rev. Mod. Phys.* **86**(2), 361 (2014).
- <sup>23</sup>L. Petit, J. Boter, H. Eenink, G. Droulers, M. Tagliaferri, R. Li, D. Franke, K. Singh, J. Clarke, R. Schouten *et al.*, “Spin lifetime and charge noise in hot silicon quantum dot qubits,” *Phys. Rev. Lett.* **121**(7), 076801 (2018).
- <sup>24</sup>S. Ahn, S. Das Sarma, and J. Kestner, “Microscopic bath effects on noise spectra in semiconductor quantum dot qubits,” *Phys. Rev. B* **103**(4), L041304 (2021).
- <sup>25</sup>M. M. E. K. Shehata, G. Simion, R. Li, F. A. Mohiyaddin, D. Wan, M. Mongillo, B. Govoreanu, I. Radu, K. De Greve, and P. Van Dorpe, “Modeling semiconductor spin qubits and their charge noise environment for quantum gate fidelity estimation,” *Phys. Rev. B* **108**(4), 045305 (2023).
- <sup>26</sup>P. Dutta and P. Horn, “Low-frequency fluctuations in solids: If noise,” *Rev. Mod. Phys.* **53**(3), 497 (1981).
- <sup>27</sup>J. H. Davies, *The Physics of Low-Dimensional Semiconductors: An Introduction* (Cambridge University Press, 1998).
- <sup>28</sup>D. Culcer, X. Hu, and S. Das Sarma, “Dephasing of Si spin qubits due to charge noise,” *Appl. Phys. Lett.* **95**(7), 073102 (2009).
- <sup>29</sup>S. Das Sarma, X. Wang, and S. Yang, “Hubbard model description of silicon spin qubits: Charge stability diagram and tunnel coupling in Si double quantum dots,” *Phys. Rev. B* **83**(23), 235314 (2011).

- <sup>30</sup>L. D. Landau and E. M. Lifshitz, *Quantum Mechanics: Non-Relativistic Theory* (Elsevier, 2013), Vol. 3.
- <sup>31</sup>T. Meunier, V. E. Calado, and L. M. Vandersypen, “Efficient controlled-phase gate for single-spin qubits in quantum dots,” *Phys. Rev. B* **83**(12), 121403 (2011).
- <sup>32</sup>D. M. Zajac, A. J. Sigillito, M. Russ, F. Borjans, J. M. Taylor, G. Burkard, and J. R. Petta, “Resonantly driven CNOT gate for electron spins,” *Science* **359**(6374), 439–442 (2018).
- <sup>33</sup>P. Huang, N. M. Zimmerman, and G. W. Bryant, “Spin decoherence in a two-qubit CPHASE gate: The critical role of tunneling noise,” *npj Quantum Inf.* **4**(1), 62 (2018).
- <sup>34</sup>F. Martins, F. K. Malinowski, P. D. Nissen, E. Barnes, S. Fallahi, G. C. Gardner, M. J. Manfra, C. M. Marcus, and F. Kuemmeth, “Noise suppression using symmetric exchange gates in spin qubits,” *Phys. Rev. Lett.* **116**(11), 116801 (2016).
- <sup>35</sup>T. Wu and J. Guo, “A multiscale simulation approach for germanium-hole-based quantum processor,” *IEEE Trans. Comput.-Aided Des. Integr. Circuits Syst.* **42**(1), 257–265 (2023).
- <sup>36</sup>D. Culcer and N. M. Zimmerman, “Dephasing of Si singlet–triplet qubits due to charge and spin defects,” *Appl. Phys. Lett.* **102**(23), 232108 (2013).
- <sup>37</sup>D. Reilly, J. Taylor, E. Laird, J. Petta, C. Marcus, M. Hanson, and A. Gossard, “Measurement of temporal correlations of the Overhauser field in a double quantum dot,” *Phys. Rev. Lett.* **101**(23), 236803 (2008).
- <sup>38</sup>D. Zajac, T. Hazard, X. Mi, E. Nielsen, and J. R. Petta, “Scalable gate architecture for a one-dimensional array of semiconductor spin qubits,” *Phys. Rev. Appl.* **6**(5), 054013 (2016).
- <sup>39</sup>J. S. Rojas-Arias, A. Noiri, P. Stano, T. Nakajima, J. Yoneda, K. Takeda, T. Kobayashi, A. Sammak, G. Scappucci, D. Loss, and S. Tarucha, “Spatial noise correlations beyond nearest neighbors in <sup>28</sup>Si/Si-Ge spin qubits,” *Phys. Rev. Appl.* **20**(5), 054024 (2023).